

MRI brain tumor detection using deep learning and machine learning approaches

Shenbagarajan Anantharajan^{a,*}, Shenbagalakshmi Gunasekaran^a, Thavasi Subramanian^a, Venkatesh R^b

^a Mepco Schlenk Engineering College, Sivakasi - 626005, Virudhunagar, Tamilnadu, India

^b Ramco Institute of Technology, Rajapalayam - 626117, Virudhunagar, Tamilnadu, India

ARTICLE INFO

Keywords:
 Brain tumour
 Magnetic resonance imaging (MRI)
 Deep learning(DL)
 Machine learning(ML)
 Adaptive contrast enhancement algorithm (ACEA)
 Gray-level co-occurrence matrix (GLCM)
 Ensemble deep neural support vector machine (EDN-SVM)

ABSTRACT

The development of aberrant brain cells, some of which may become cancerous, is known as a brain tumour. The quality of life and life expectancy of patients are enhanced by early and timely illness identification and treatment plans. Magnetic Resonance Imaging (MRI) scans are the most common approach for finding brain tumors. However, the ability of radiologists and other clinical experts to identify, segment, and remove contaminated tumour regions from MRI images is a critical factor in a process that is iterative and labor-intensive and relies on those individuals' abilities in these areas. Concepts for image processing may envision the diverse human organ anatomical structures. It is difficult to find abnormal brain regions using simple imaging methods. Over the last several years, interest in the emerging machine learning field of "Deep Learning (DL)" has grown significantly. It was extensively used in numerous applications and shown to be an effective Machine Learning (ML) technique for many of the challenging issues. This research suggests a novel MRI brain tumour detection method based on DL and ML. Initially the MRI images are collected and preprocessed using Adaptive Contrast Enhancement Algorithm (ACEA) and median filter. Fuzzy c-means based segmentation is done to segment the preprocessed images. The features like energy, mean, entropy and contrast are extracted using Gray-level co-occurrence matrix (GLCM). The abnormal tissues are classified using the proposed Ensemble Deep Neural Support Vector Machine (EDN-SVM) classifier. The numerical findings reveal a better accuracy (97.93 %), sensitivity (92 %), and specificity (98 %) in recognizing aberrant and normal tissue from brain MRI images, which supports the effectiveness of the approach that was recommended.

1. Introduction

The human brain is regarded to be one of the most essential organs since it is responsible for a large number of the body's regulatory processes, including memory, emotions, vision, motor skills, responses, and breathing. In the event that a tumour begins to form inside the brain, these functions will be significantly disrupted [1,3]. This tumour is either a primary brain tumour (BT), which develops from inside the brain itself and represents the development of brain tissues themselves, or it is a metastatic BT, which develops in another part of the body and eventually spreads to the brain. When compared to tumors that originate in any other organ of the human body, those that occur in the brain provide a significant diagnostic challenge. Because the brain has the "Blood-Brain Barrier (BBB)", ordinary radioactive markers are unable to

detect the hyperactivity of tumour cells in the body [2]. Consequently, MRI scans are considered to be the most effective diagnostic tracers for detecting breaches in the BBB. Fig. 1(A) and (B) depicts the images of healthy brain and tumour brain.

There are between 7 and 11 cases of brain tumors per 100,000 people in various age groups per year. It is estimated that 227,000 people die each year as a result of this dreadful illness. In addition, about 7.7 million survivors are adjusting to life with a disability [4]. As well as saving lives, an early diagnosis of a brain tumour may help prevent disability. The brain, the body's most delicate organ, will be subjected to less modification and surgery if it is detected early. To begin with, a radiologist will need to take a picture of the affected area in order to do a manual diagnosis [5]. After that, an experienced physician is consulted for the purpose of image analysis and the formulation of a treatment

* Corresponding author.

E-mail addresses: asrme2008@gmail.com (S. Anantharajan), pri.infotech@gmail.com (S. Gunasekaran), sktthavasi@gmail.com (T. Subramanian), venkey88me@gmail.com (V. R.).

strategy. Unfortunately, the research that investigated the accuracy of manually diagnosing brain tumors reported a discrepancy amongst the experts who reviewed the data. According to reports, the level of agreement amongst specialists for the manual diagnosis of a BT is between 90 and 95%. The degree of disagreement amongst the specialists is further reduced when it comes to mixed types of tumour, mixed glioma, and medulloblastoma, falling to 77 % and 58 %, respectively [6].

Digital image processing and other advancements in medical imaging have contributed to the widespread use of computer-aided diagnosis (CAD) in recent years. The MRI technique is favoured for use in diagnostic systems like these since it does not pose a threat from ionising radiation and is able to reliably identify blood flow in veins [7]. The use of large medical image datasets, such as Brain MRI scans, for the identification of BT may be aided by the use of ML and DL algorithms. Creating a ML and DL model is a multistep process that involves training using a significant quantity of medical imaging data [8]. This is necessary in order to get the correct prediction or insight from the model, which is necessary in order to make an appropriate clinical decision. In this study, we investigate the identification of brain tumors using DL and ML techniques.

The major contributions of this study are as follows.

- To preprocess the MRI images, Adaptive Contrast Enhancement Algorithm (ACEA) and median filter is used.
- Fuzzy c-means based segmentation is done to segment the pre-processed images.
- The features are extracted using GLCM approach.
- The abnormal tissues are classified using the proposed EDN-SVM classifier.

The study is structured in such a manner that Section 2 provides related work and problem statement, Section 3 outlines the recommended approach, Section 4 depicts findings and discussion, and Section 5 draws a conclusion to the research along with the future work that will be done.

2. Related WORKS

The author of [9] suggested method identifies the kind of tumors present in the BT MRI image and marks the tumour region. Alex Net model and the Faster R-CNN algorithm's Region Proposal Network (RPN) are utilised as the basic models for classifying various tumour kinds. The study [10] employed a Deep NN classifier, a component of the deep learning designs, to divide 66 brain MRI scans into four categories, including "normal", "glioblastoma", "sarcoma", and "metastatic bronchogenic carcinoma tumors". The author of [11] constructed brain MRI images were utilised to create a Convolutional Neural Network (CNN) to identify a tumour. In Ref. [12], the author used a CNN-based

methodology as well as a deep neural network technique to categorise an MRI as "tumour detected" or "tumour not detected." The study [13] showed the promise of DL in MRI scans as a non-invasive method for simultaneous and automated tumors segmentation, identification, and grading of LGG in clinical settings. The research [14] presents a faster and more accurate method for detecting human brain cancers by combining the "Template-based K-means (TK)" algorithm with pixels in the image and "Principal Components Analysis (PCA)".

The "Watershed Dynamic Angle Projection - Convolution Neural Network (WDAPP-CNN)" is able as a nation method for tumors identification in this research [15]. The tumors area was successfully segmented using the watershed technique. The research [16] suggested technique guarantees to be very effective and exact for detecting, classifying, and segmenting brain tumors. Automated segmentation is performed on image data using a CNN-based method, which employs very small kernel sizes of 33. The author of [17] focused early identification of benign brain tumors. Segmentation is required in the early stages of brain tumors identification. Algorithms usually for segmentation have several limitations, including the inability to handle noisy data and the inability to identify subtle intensity variations in the image. The study of [18] presented a comprehensive and entirely automated MRI brain tumors identification and segmentation approach employing the "Gaussian mixture model", "Fuzzy C-Means", "active contour", "wavelet transform", and "entropy segmentation" techniques as an effective clinical-aided tool. The two key components of the suggested approach are tumors auto-detection and segmentation as well as skull removal. The research [19] suggested approach tries to distinguish between BT and normal brains. Brain magnetic resonance imaging is used to research various forms of brain malignancies. Support vector machines and various wavelet transformations are used to identify and categorise MRI brain cancers. The Study [20] proposed hybrid K-means Galactic Swarm Optimization (GSO) technique is adopted as a practical solution to the image segmentation issue, which is considered as a classification model. Study developed a Fuzzy C-Means clustering technique, which was followed by conventional detectors and CNN to remove brain tumors from 2D MRI. The experiment utilised real-time dataset with various tumors sizes, locations, forms, and image brightness. The author of [21] presented a comprehensive assessment of the literature on current approaches to segmenting BT from brain MRI data. The author of [26] provided a thorough critique of the research and discoveries made in the recent past to identify and categorise brain tumors using MRI scans. Researchers that specialize in deep learning and are interested in using their knowledge for the identification and classification of brain tumors may particularly benefit from this work. According to the study [27] an automated approach is offered to distinguish between malignant and non-cancerous brain MRI scans by Using three benchmark datasets, the suggested technique is verified, with average results of 97.1 % accuracy, 0.98 area under the curve, 91.9 % sensitivity, and 98.0 %

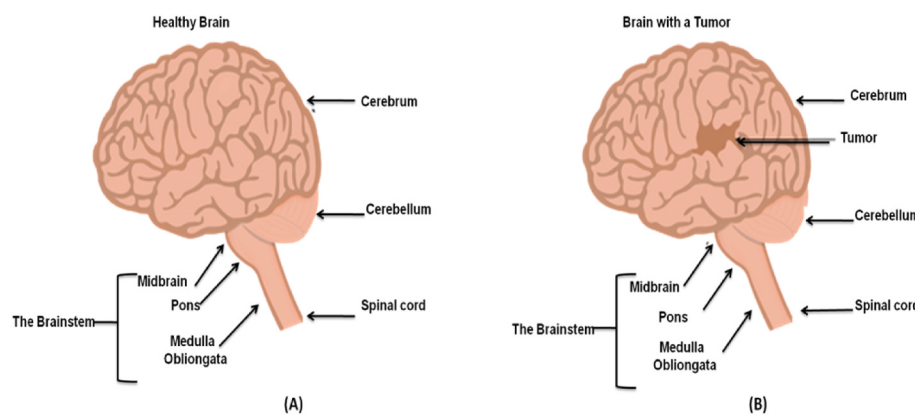


Fig. 1. Image of (A) Healthy brain (B) Brain with a tumour.

specificity. Compared to current techniques, it can be utilised to detect the tumour more precisely and with less processing time. The study [28] proposes a two-step Dragonfly algorithm (DA) clustering method to precisely extract starting contour points. At the preprocessing stage, the brain is removed from the skull. Then, tumour edges are extracted using the two-step DA, and these extracted edges are utilised as a starting contour for the MRI sequence.

2.1. Problem statement

Brain tumors have the potential to generate consequences such as physical impairments, which would then need patients to undergo very intensive therapy, which is often rather painful, in order to cure or lessen the caused disabilities. In addition, the negative effects that brain tumors have on the functioning of the brain might vary depending on the size of the tumour, where it is located, and what kind it is. Because a tumour might exert pressure on the region of the brain that regulates the body's mobility, the patient can become immobile as a result of this. If it is diagnosed sooner, it may be possible to prevent disability from occurring. There are a number of obstacles that need to be overcome in order to correctly categorise brain tumors. These obstacles include the fact that brain tumors exhibit a high degree of variation with regard to their size, shape, and intensity, and that tumors of different pathological types may have similar outward appearances.

3. Proposed methodology

This section provides a comprehensive discussion of the identification of MRI brain tumors utilizing both DL and ML techniques. The progression of the recommended technique is shown in Fig. 2. In the beginning, MRI brain tumour data were obtained and preprocessed with the help of ACEA and the median filter in order to get rid of the noise. In order to segment the MRI brain images, a fuzzy c-means technique is

applied, and a GLCM matrix is used to extract the features of the images. The EDN-SVM approach is then used to classify the images of healthy and tumorous brain tissue.

3.1. Dataset collection

We utilize a dataset that may be found on the Kaggle open data website in order to evaluate the performance of the suggested architectural design. This dataset includes 255 T1-mode MRI images. It includes 98 MRI slices taken from healthy brain tissue and 155 MRI slices taken from tumorous brain tissue. Because each of these images had a unique dimension, we needed to adjust it so that it would fit inside the parameters of our image requirements. A portion of the dataset that we used for our investigation is shown in Fig. 3(A). It depicts that the width and height of the images vary from one another. When looking at MRI brain scans with various heights and widths, it might be difficult to appropriately classify healthy brain tissue and tumorous brain tissue. As a consequence of this, before moving on to the preprocessing stage, we resize the images such that their width and height are the same. The scaled versions of the images from the dataset are shown in Fig. 3(B).

3.2. Preprocessing

3.2.1. Adaptive contrast enhancement algorithm

MRI image contrast is crucial for tumour identification since this technique relies heavily on image brightness. The two typical histograms for MRI scans are high contrast and low contrast. A piecewise linear histogram modification is often used to improve intensity contrast. Because the transformation slope varies from one set of data to another, it is difficult to establish universal minimum and maximum values that apply to all images. Here, we use an automated and dynamic method to extract the parameters from each image. A brain tumour (T), healthy brain tissue (B), and vessels (V) can all be distinguished in an

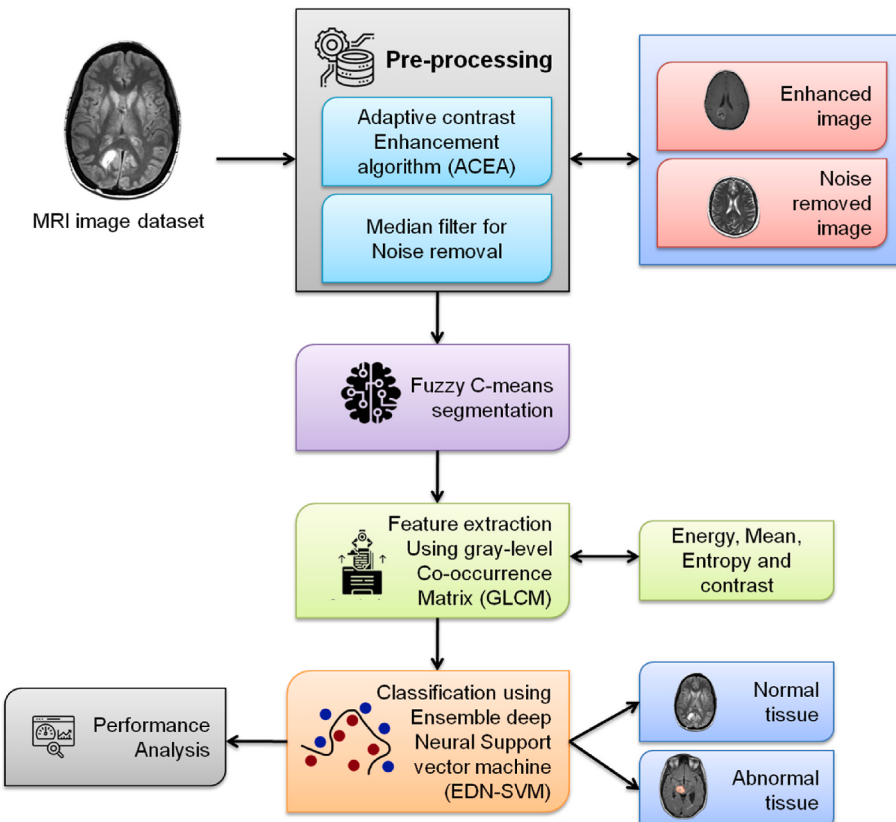


Fig. 2. Workflow of the proposed technique.

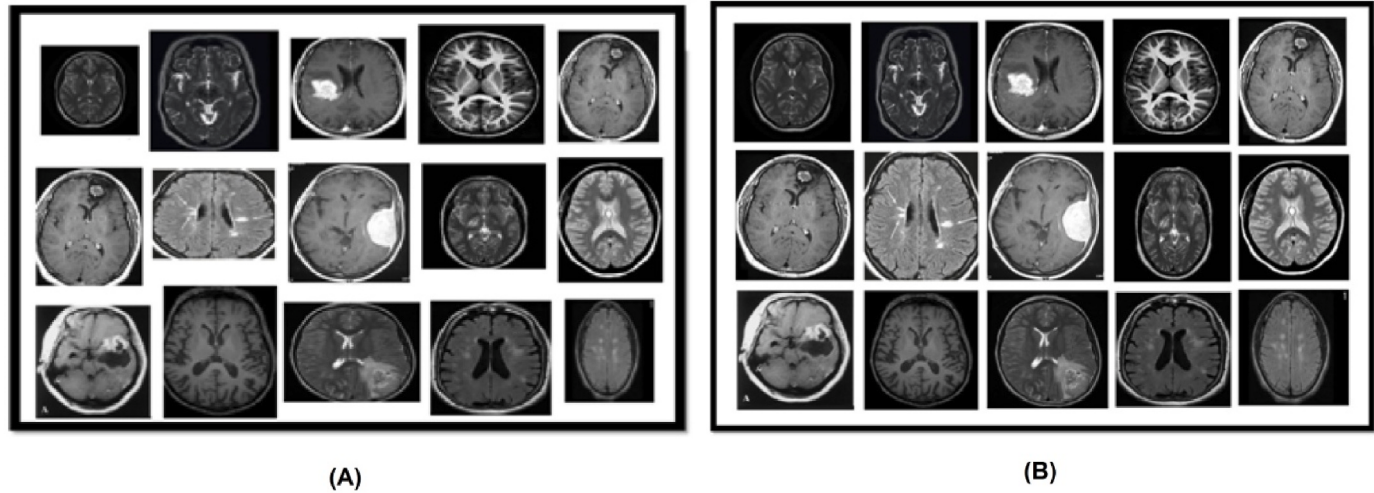


Fig. 3. Sample dataset images of (A) varying size (B) same size.

MRI scan of the head. To begin, we take the training data and choose some random voxels to represent each of the three classes. It is hypothesized what the intensity probability distribution function (PDF) looks like for each category.

In addition to averaging their values ($\mu_T^Z, \mu_B^Z, \mu_V^Z$), and calculating their standard derivations ($\sigma_T, \sigma_B, \sigma_V$), we additionally calculate the highest PDF intensity value for the brain class, N^Z . The mean value have the $\mu_T^Z < \mu_B^Z < \mu_V^Z$ characteristic. While mean and derived values may vary from image to image, the normal brain always has a higher mean value than the tumour and a lower mean value than the blood vessels. One may use this to divide things up into three categories and we name it Curve Pattern Z. First, we determine the intensity PDF of a brand-new image, using the segmented brain volume as input. We find the volume of the new brain that corresponds to the maximum probability density N^V of the probability density function (PDF). Healthy tissues dominate volume, therefore this assumption is reasonable. We may determine the mean intensity values of the other two classes by adjusting the three curves in Curve Pattern Z. Tumour mean value and vessel values are $\mu_T = N^V - N^Z + \mu_T^Z$ and $\mu_V = N^V - N^Z + \mu_V^Z$. All three classes employ conventional derivations. Set the lower limit as $P_{min} = \mu_T - 3\sigma_T$ and the upper limit as $P_{max} = \mu_V + 3\sigma_V$. The formula for intensity transform of range 0–255 is given in equation (1). The formula is

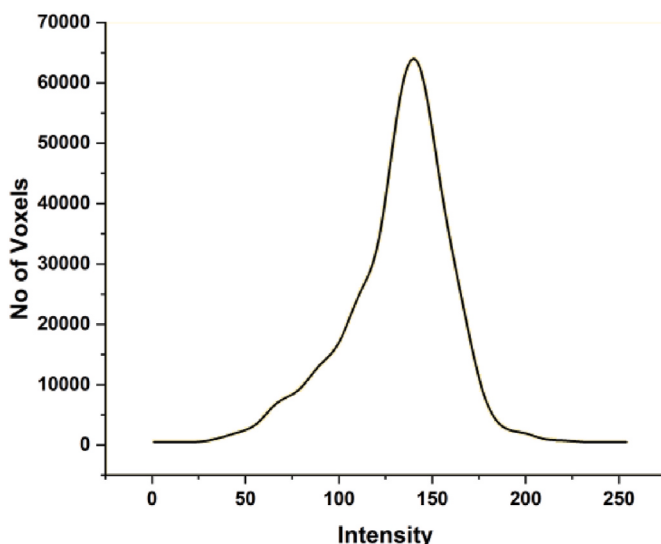


Fig. 4. Transformation histogram.

used to re-estimate the intensity histograms of brain images (Fig. 4).

$$\begin{cases} \frac{(I_x - P_{min})}{(P_{max} - P_{min})}(255 - 1) + 1 & \text{if } (P_{min} \leq I_x \leq P_{max}) \\ 0 & \text{if } (I_x < P_{min} \cup I_x > P_{max}) \end{cases} \quad (1)$$

$P_{min} : \mu_{tumor} - 3\sigma, P_{max} : \mu_{vessel} + 3\sigma$

3.2.2. Median filter

When applied to MRI scans of the brain, this nonlinear technique effectively eliminates unwanted background noise. Edge preservation with this approach is common practise. Salt and pepper noise may be eliminated with great success. Median filter is similar to mean filter in that it iteratively processes an image, but it replaces each pixel's value with the middle value of its neighbours rather than the mean. After sorting all the neighbouring pixel values into numerical order, the median pixel value from the neighbouring pixel values is used to replace the pixel under consideration. When it comes to decreasing noise without diminishing image quality, the median filter is much superior.

$$c(i,j) = \text{median}_{(o,b) \in G_{ij}} \{k(o,b)\} \quad (2)$$

where G_{ij} denotes the sets of coordinates centred on the coordinates (i,j) within the rectangle sub image frame, and median is the median value inside the window. To demonstrate how effective the noise reduction approach is, we apply it to the noisy picture and the result is presented in Fig. 5.

3.3. Fuzzy C-means (FCM) segmentation

The process of image segmentation benefits greatly from the use of fuzzy clustering. An efficient approach that may be used in fuzzy clustering is known as the fuzzy c-means algorithm. The FCM is a clustering approach that makes it possible for a single pixel to belong to many clusters at the same time. The FCM method makes an effort to divide a finite collection of pixels into a collection of "C" fuzzy clusters by applying certain supplied criteria to the decision-making process. The FCM method seeks to achieve the lowest possible value for the objective function shown below

$$Y(O, f_1, f_2, \dots, f_f) = \sum_{x=1}^f Y_x = \sum_{x=1}^f = \sum_{y=1}^m o_{xy}^n s_{xy}^2 \quad (3)$$

s_{xy} is the Euclidean distance between the x th centroids and y th data point. $nF [1, \infty]$ is a weighting function. o_{xy} is between 0 and 1. An

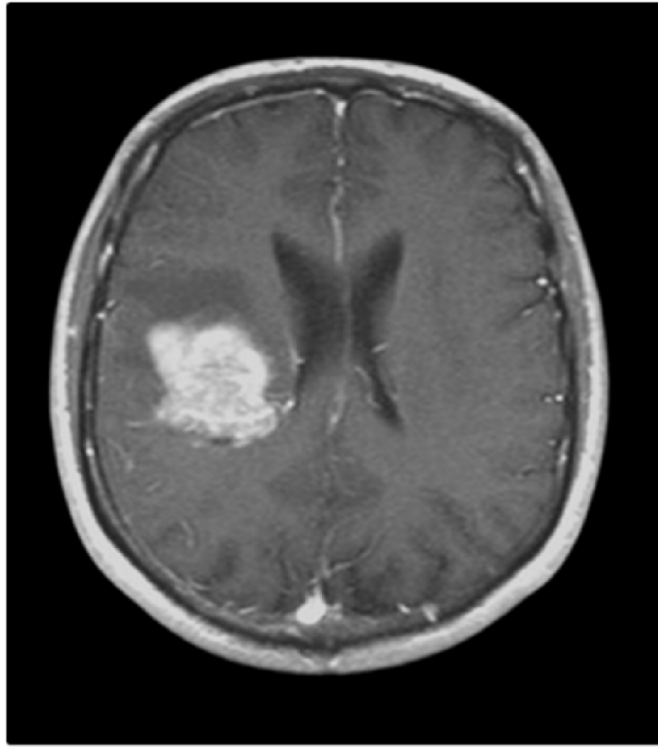


Fig. 5. Noise removed image using median filter method.

iterative optimization of the objective function is used to accomplish fuzzy portioning of known data samples.

$$o_{xy} = \frac{1}{\sum_{g=1}^f \left(\frac{s_{xy}}{s_{gy}} \right)^{(2/n-1)}} \quad (4)$$

$$f_y = \frac{\sum_{y=1}^m o_{xy}^n i_y}{\sum_{y=1}^m o_{xy}^n} \quad (5)$$

The iteration will end when $\max_{xy} \{|o_{xy}^{(g+1)} - o_{xy}^{(g)}|\} < \epsilon$, where ϵ is a termination condition between 0 and 1, and g is the iteration steps. The method approaches a local minimum or a saddle point of y_n . **Fig. 6** depicts the MRI brain image after segmentation. Here are the individual components that make up the algorithm:

1. Initialize $O = [o_{xy}]$ matrix, $O^{(0)}$.

2. At k-step: calculate the centers vectors $F^{(g)} = [f_y]$ with $O^{(g)}$.

$$f_y = \frac{\sum_{x=1}^M o_{xy}^n i_x}{\sum_{x=1}^M o_{xy}^n} \quad (6)$$

Update $O^{(g)}, O^{(g+1)}$.

$$o_{xy} = \frac{1}{\sum_{g=1}^f \left(\frac{\|i_x - f_y\|}{\|i_x - f_g\|} \right)^{\frac{2}{n-1}}} \quad (7)$$

If $\|O^{(g+1)} - O^{(g)}\| < \epsilon$ then STOP; otherwise return to step 2.

D. Feature extraction using Gray level Co-occurrence matrix (GLCM).

The GLCM technique is used in order to extract the image features in this approach. A statistical approach known as the co-occurrence matrix is used to a particular brain image in order to extract the second order statistical textural qualities. When using GLCM, the number of gray levels must always be equal to the number of rows and columns. The following equations are used to extract the characteristics that are based on the first order of the histogram. In the approach that was suggested, shape, textural, and statistical characteristics are taken from each cluster, and then these features are supplied to the classifier so that it can locate the tumors in the MRI image that was provided. The following are the extracted features:

$$\text{Entropy} = \sum_{x=0}^{m-1} \sum_{y=0}^{m-1} T_{xy} \log T_{xy} \quad (8)$$

A random variable's entropy may be thought of as a measurement of its degree of uncertainty. When all of the components of the co-occurrence matrix are the same, its value will be at its highest possible level.

$$\text{Correlation} = \frac{\sum_{x=0}^{m-1} \sum_{y=0}^{m-1} (x, y) t(x, y) - \mu_i \mu_j}{\sigma_i \sigma_j} \quad (9)$$

The correlation metric determines how closely connected the reference pixel is to its neighbouring pixel.

$$\text{Energy} = \sum_{x=0}^{m-1} \sum_{y=0}^{m-1} T_{xy}^2 \quad (10)$$

Energy is the metric used to define the sum of squared components. This determines how homogenous the mixture is. When pixels are substantially comparable to one another, the energy value will be high.

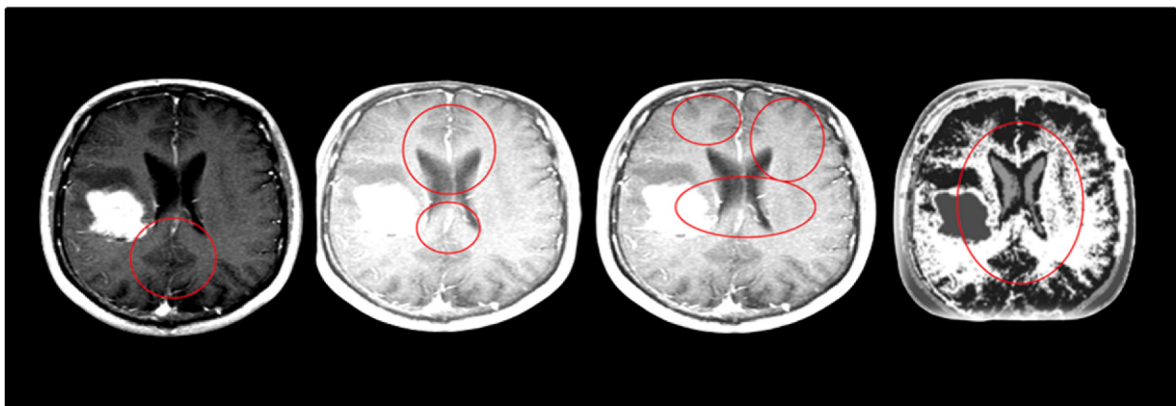


Fig. 6. MRI brain image after FCM approach.

$$\text{Contrast} = \sum_{m=0}^{mk-1} m^2 \sum_{x=0}^{mk-1} \sum_{y=0}^{mk-1} T(x, y)^2 \quad (11)$$

The contrast of an image is the difference in brightness between the reference pixel and its neighbouring pixel.

$$\text{Mean } (\mu) = \sum_{x=0}^{mk-1} x \cdot t(x) \quad (12)$$

The average amount of brightness of an image or texture is described by its mean. Around the mean, the variance characterises the range of values in terms of their relative intensity.

$$\text{Standard Deviation } (\sigma) = \sqrt{\sum_{x=0}^{mk-1} (x - \mu)^2 \cdot t(x)} \quad (13)$$

$$\text{Variance } (\sigma^2) = \sum_{x=0}^{mk-1} (x - \mu) \cdot t(x) \quad (14)$$

3.4. Classification using ensemble deep Neural Support Vector Machine (EDN-SVM)

In this paper, we introduce the Neural Support Vector Machine (NSVM), a hybrid machine learning algorithm consisting of both neural networks and SVMs. The output of the NSVM is given by support vector machines that take a small central feature layer as their input. This feature layer is in turn the output of a number of neural networks, trained through backpropagation of the derivatives of the dual objectives of the SVMs with respect to the feature-node values. The NSVM aims to overcome the problems of the standard SVM. First, the NSVM adds more layers to the SVM, making it “deeper”. Furthermore, the neural networks can learn arbitrary features, making the kernel functions much more flexible. Finally, by combining multiple SVMs with a shared feature layer into one learning architecture, the NSVM extends an SVM’s generalization capability to multiple outputs.

We introduced a novel hybrid approach termed as Ensemble Deep Neural Support Vector Machine (EDN-SVM) for classification. This algorithm is comprised of both NNs and SVMs. SVMs accepted the dimensionally reduced central features to provide the output of the EDN-SVM. To train the EDN-SVM, significant feature layer is utilised. As a result of being trained by backpropagation of the derivatives of the dual goals of the SVMs with regard to the values of feature-node, a number of NNs produce this feature layer as their output. The shortcomings of the conventional SVM are targeted for improvement by the EDN-SVM. To begin, the EDN-SVM is able to “deepen” the SVM by adding more layers to it. In addition, the NN is able to learn completely arbitrary characteristics, which makes the kernel functions far more adaptable. In conclusion, the EDN-SVM is able to expand the generalization power of an SVM to multiple outputs. This is accomplished by merging several SVMs with a shared feature layer into a single learning architecture.

3.4.1. Support vector regression (SVR)

The training for linear ξ insensitive SVR consists of finding the optimal solution to the following restricted optimization problem:

$$\min_{e, \xi^{(*)}, v} \left[\frac{1}{2} \|e\|^2 + F \sum_{x=1}^h (\xi_i + \xi_x^*) \right] \quad (15)$$

conditional on the following:

$$j_x - e \cdot I_x - v \leq +\xi_x, e \cdot I_x + v - j_x \leq +\xi_x^*, \text{ and } \xi_x, \xi_x^* \geq 0 \quad (16)$$

In this equation, e denotes the weight vector, v means the bias value, (I_x, j_x) refers to the training sample and its respective target value, ξ_x and ξ_x^* are the “slack variables” that enable the model to accommodate

discrepancies between the model’s output and the instance’s target value, a range of permissible deviations is denoted by F , and the total number of training samples is denoted by h . F is a parameter controlling the magnitude to which such deviations are allowed, and h is the total number of training samples. The terms “primal goal” and “primal variables” refer, respectively, to the variables in Equation (15). By introducing the Lagrange multipliers $\alpha, \alpha^{(*)}$ and solving for the saddle point’s coordinates, we may rewrite the original goal and constraints as follows.

$$\begin{aligned} \max_{\alpha^{(*)}} \quad & \left[-v \sum_{x=1}^h (\alpha_x^* + \alpha_x) + \sum_{x=1}^h (\alpha_x^* - \alpha_x) j_x \right. \\ \alpha^{(*)} \quad & \left. - \frac{1}{2} \sum_{x,y=1}^h (\alpha_x^* - \alpha_x) (\alpha_y^* - \alpha_y) (I_x - I_y) \right] \end{aligned} \quad (17)$$

conditional on the following:

$$0 \leq \alpha_x^{(*)} \leq F \quad \text{and} \quad \sum_{x=1}^h (\alpha_x - \alpha_x^*) = 0 \quad (18)$$

Here, $\alpha_x^{(*)}$ stands in for α_x and α_x^* , whereas $\alpha^{(*)}$ represents the vectors that include all α_x^* values. The term “dual objective” refers to Equation (17). “Bias constraint” refers to the second constraint in Equation (18). Finding the α and $\alpha^{(*)}$ that maximises the dual goal is the first step in a linear regression SVM’s determination of its output.

$$c(i) = \sum_{x=1}^h (\alpha_x^* - \alpha_x) (I_x \cdot I) + v \quad (19)$$

A linear relationship between I_x and I is assumed in the provided SVR model. Obviously, we need a nonlinear version of the SVR model. To achieve this, we may utilize a map to convert the training patterns I_x into a higher-dimensional feature space, and then run the data through the standard SVR method. However, this strategy may quickly become computationally impossible. It is sufficient to know that $g(I_x, I) := \psi(I_x) \cdot \psi(I)$, in order to get the regression estimate and the dual goal, respectively. In order to make SVR nonlinear, this kernel function is often used. Several types of kernel functions, including as radial basis functions, polynomial functions, and sigmoidal functions, have extensive use.

3.4.2. Ensemble deep Neural Support Vector Machine (EDN-SVM)

There are four parts to the EDN-SVM, as shown in Fig. 7: (1) an input layer with S nodes, (2) a central feature layer with s nodes, (3) a sum of s two-layer NNs (MLPs) M each one capture the full input layer as input and produce one of the attribute values, and (4) a main support vector regression model N that takes the entire feature layer as input and determines the output node value. After receiving a pattern x in dimension S , the EDN-SVM sends it on to the NNs, where it is transformed into a vector that becomes the basis for the feature layer’s values. As a shorthand for the mapping that the NNs produce, we use $\varphi(I|\theta)$, and we represent the NNs’ weights as a vector. The value of the output node is calculated using the support vector machine M , which takes as input the representation in the feature layer. In order to arrive at its conclusion, the regression EDN-SVM uses:

$$C(i) = \sum_{x=1}^h (\alpha_x^* - \alpha_x) g(\varphi(I_x|\theta), \varphi(I|\theta)) + v \quad (20)$$

This is the primary SVM kernel function, which is denoted by $g(\cdot, \cdot)$. As shown in Fig. 7, the EDN-SVM estimator has the following architectural layout. Three separate neural networks, each extracting a different feature, make up the feature layer in this example.

3.4.3. Modified objectives

Finding an acceptable value for the variable c requires the system to learn a representation of the input MRI brain data in ‘a’ that codes the properties that are most relevant for computing the desired output. The

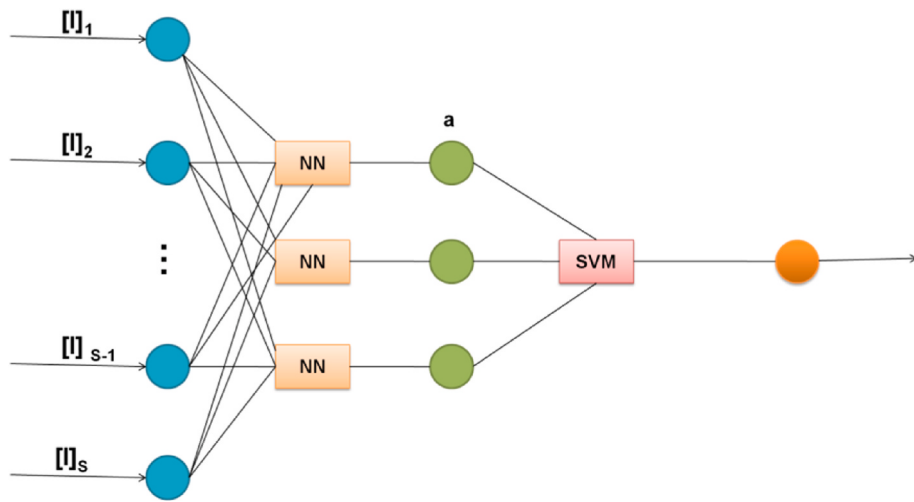


Fig. 7. Architecture of END-SVM estimator.

fundamental goal of SVR is modified by the EDN-SVM, which does this by exchanging the training samples I_x for their representation in the feature layer. As a consequence of this, the weight vector of the NNs θ is included as an extra primary variable. This results in the following primary goal for an EDN-SVM when using a linear SVR model N:

$$\min_{e, v, \theta} \left[\frac{1}{2} \|e\|^2 + F \sum_{x=1}^h (\xi_i + \xi_x^*) \right] \quad (21)$$

The new ‘dual objective’ for the EDN-SVM when the SVR system N utilises a kernel function $K(\cdot, \cdot)$ is, in accordance, as follows:

$$\begin{aligned} \min_{\theta} \max_{\alpha^{(*)}} E(\alpha^{(*)}, \theta) = & -\varepsilon \sum_{x=1}^h (\alpha_x^* + \alpha_x) + \sum_{x=1}^h (\alpha_x^* - \alpha_x) j_x \\ & - \frac{1}{2} \sum_{x,y=1}^h (\alpha_x^* - \alpha_x)(\alpha_y^* - \alpha_y) G(\varphi(I_x|\theta), \varphi(I_y|\theta)) \end{aligned} \quad (22)$$

conditional on the following:

$$0 \leq \alpha_i, \alpha_x^* \leq F, \text{ and } \sum_{x=1}^h (\alpha_x^* - \alpha_x) = 0 \quad (23)$$

3.4.4. Training procedure

The training of the EDN-SVM estimator has two primary objectives: (1) Determine the value of $\alpha^{(*)}$ that maximises Equations (22), and (16). Determine the values of the weights of the NNs θ in such a way that each network M_α contributes to the I_x that minimises Equation (22). Both of these objectives cannot be accomplished in isolation; rather, in order to adjust, it is necessary to also alter the NNs, and vice versa. Whenever the model is shown a training pattern I_x , the END-SVM employs a gradient ascent method to make adjustments to each α_x and $\alpha_x^{(*)}$ in the direction of a local maximum of $E(\cdot, \cdot)$:

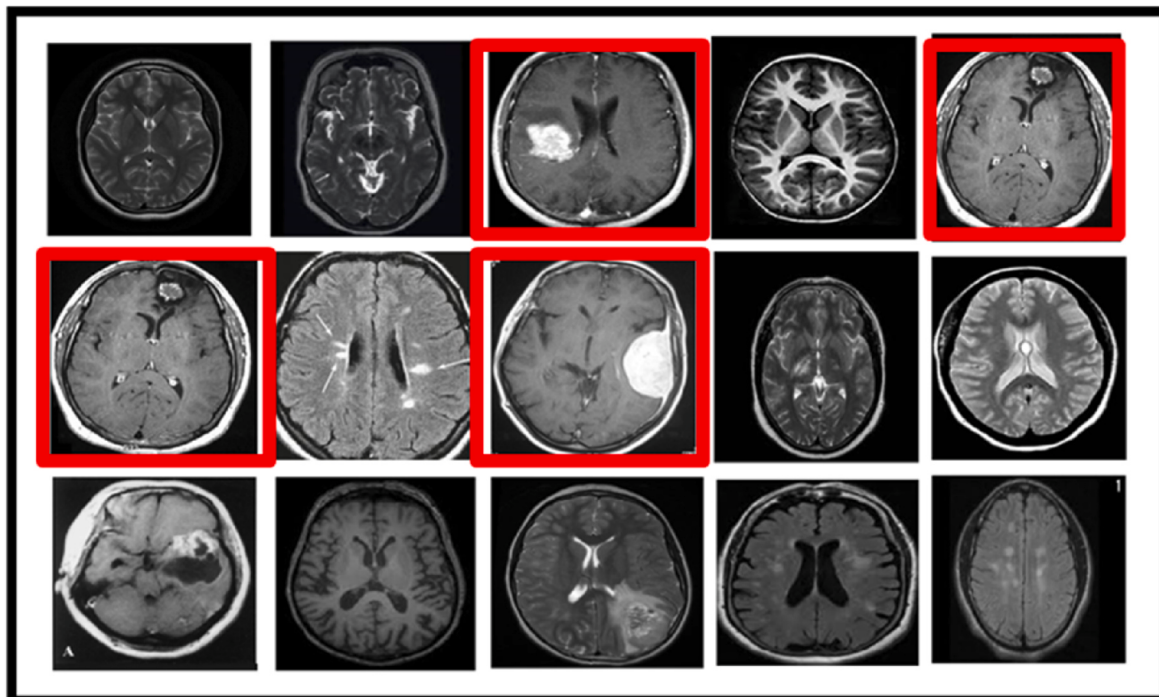


Fig. 8. Tumour identification after EDN-SVM approach.

$$\alpha_x^{(*)} \leftarrow \alpha_x^{(*)} + \lambda \frac{\partial e + (\cdot)}{\partial \alpha_x^{(*)}} \quad \text{with} \quad E^+(\cdot) = E(\cdot) - T_1 \left(\sum_{y=1}^h (\alpha_y^* - \alpha_y) \right)^2 - T_2 \alpha_x^* \alpha_x \quad (24)$$

where λ is a metaparameter that controls the learning rate, and T_1 and T_2 are parameters that are decided upon in advance. With the use of the derivative of $E^+(\cdot)$ in Equation (24), we can make sure that $\alpha_x^{(*)}$ is modified such that the bias requirement holds true and that the pair $(\alpha_x^{(*)}, \alpha_x)$ has at least one value equal to zero. The following are the two expressions that represent the derivatives of our gradient ascent algorithm:

We maintain all $\alpha^{(*)}$ coefficients between 0 and F. It is our goal to modify the weights of each NN M_α in such a way that its output results in the lowest possible value of $E^+(\cdot)$. We will refer to the output of M_α given training pattern I_x as a a_x^* from now on. After that, we will attempt to reduce a_x^* by making use of gradient descent.

$$\frac{\partial E^+(\cdot)}{\partial a_x^*} = -(\alpha_x^* - \alpha_x) \sum_{y=1}^h (\alpha_y^* - \alpha_y) \frac{\partial G(\varphi(I_x|\theta), \varphi(I_y|\theta))}{\partial a_x^*} \quad (27)$$

Given an input pattern I_x , we may use backpropagation to reduce the error of M_α by adjusting its weights according to Equation (27). Algorithm 1 provides the whole training procedure. The results demonstrate that training the neural networks and the primary SVM are interleaved for a certain number of epochs. The average error is used to learn the SVR model N's bias value.

Algorithm 1. EDN-SVM

Algorithm 1: EDN-SVM

```

Initialize main SVM N
Initialize NNs
repeat
    Calculate kernel matrix for main SVM N
    Train main SVM N
    Use backpropagation on the dual objective of N to train the NNs
until stop condition (maximal no of epochs)

```

$$\frac{\partial E^+(\cdot)}{\partial \alpha_x^{(*)}} = -\varepsilon + j_x - \sum_{y=1}^h (\alpha_y^* - \alpha_y) G(\varphi(I_x|\theta), \varphi(I_y|\theta)) - 2T_1 \sum_{y=1}^h (\alpha_y^* - \alpha_y) - T_2 \alpha_x^* \quad (25)$$

and

$$\frac{\partial E^+(\cdot)}{\partial \alpha_x^{(*)}} = -\varepsilon - j_x + \sum_{y=1}^h (\alpha_y^* - \alpha_y) G(\varphi(I_x|\theta), \varphi(I_y|\theta)) + 2T_1 \sum_{y=1}^h (\alpha_y^* - \alpha_y) - T_2 \alpha_x^* \quad (26)$$

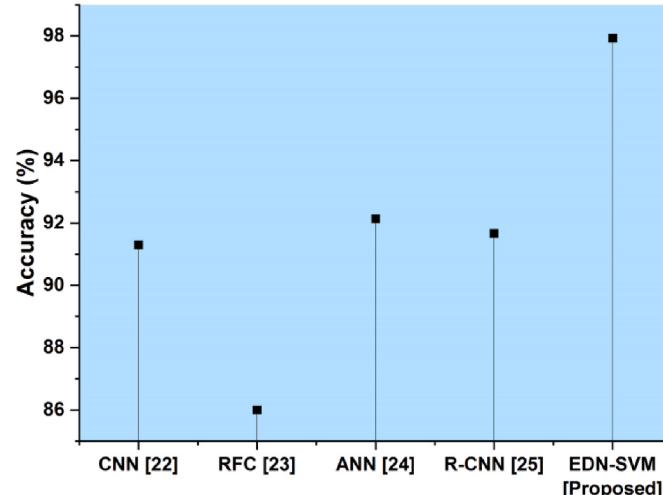


Fig. 9. Accuracy comparison.

The END-NSVM has a computational time and space complexity that scales linearly with the number of inputs and also scales linearly with the number of feature-extracting neural networks used. In the same way as SVMs do, its complexity is proportional to the amount of instances used for training.

4. Results and discussion

In this part, we will explore the identification of brain tumors by MRI utilizing both deep learning and machine learning techniques. Here we used the Python 3.7.16 version for implementation. The four basic matrices that are used in performance prediction are referred to as "True Positive (t_p)", "True Negative (t_n)", "False Positive (f_p)", and "False Negative (f_n)". In this context, cases are said to be true positives if the tumour can be accurately anticipated. Instances that may have been fairly anticipated to be negative, known as true negatives, are examined. Instances of cases that were meant to be successfully predicted but turned out to be inaccurate are examples of false positives. False negatives are situations that are meant to be mistakenly detected but are, in reality, it is properly predicted one. In addition, the accomplishments of the suggested methodology are compared with the accomplishments of existing methods such as "Convolutional neural network (CNN)", "Random Forest Classifier (RFC)", "Artificial neural network (ANN)", and "Region-based Convolutional Neural Networks (R-CNN)" in terms of "Accuracy", "Bit error rate", "Computational time", "Peak Signal Ratio", "Jaccard coefficient", "Sensitivity" and "Specificity". MRI brain tumour images may be predicted with the use of the EDN-SVM classifier model that was described before, as shown in Fig. 8.

4.1. Accuracy

Accuracy is measured by comparing the total number of MRI brain

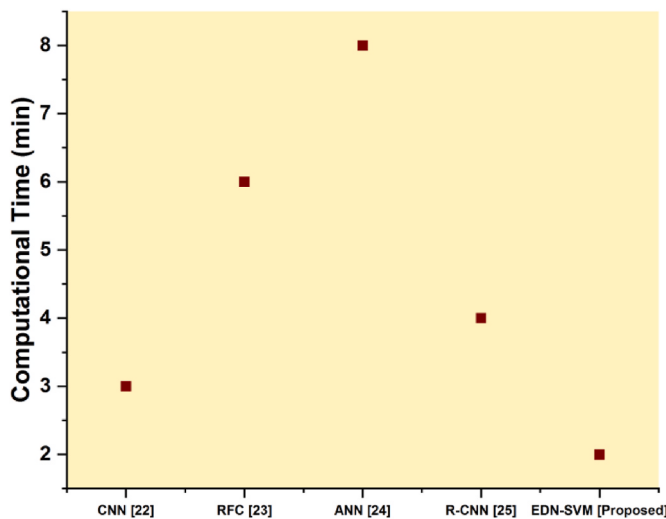


Fig. 10. Computational time comparison.

images to the number of total images and calculating the percentage of healthy and tumorous brain tissue that can be reliably predicted. The greatest consideration has been given to determining the optimal value for the evaluation parameter of the estimating classifier. The accuracy of the recommended approach is compared to that of the standard methods in Fig. 9. By computing the proportion of healthy and tumorous brain tissue, the recommended technique for classifying MRI brain pictures has a higher degree of accuracy than the traditional approaches, as is clearly evident in the figure. The proposed method has a high accuracy of 97.93 % compared with the existing methods.

$$\text{Accuracy} = \frac{t_p + t_n}{t_p + t_n + f_p + f_n} \quad (28)$$

4.2. Computational time

The amount of time needed to carry out a computing operation is referred to as the “computation time,” although it is also often termed the “running time.” Fig. 10 displays a comparison of the amount of time required to compute using the recommended technique with the time required by the conventional methods. In contrast to conventional approaches for categorising MRI images, the recommended method EDN-SVM computes the detection in less time, as seen by the figure.

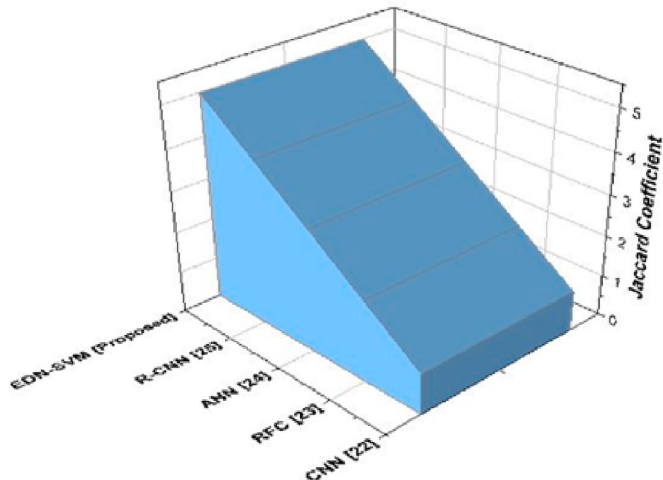


Fig. 11. Jaccard coefficient.

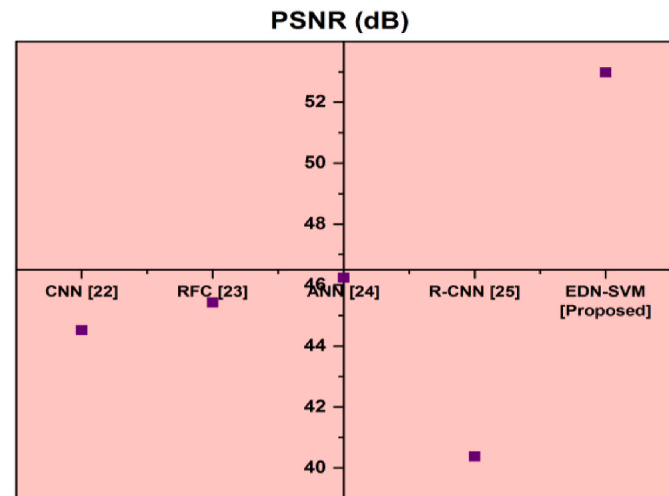


Fig. 12. Psnr comparison.

4.3. Jaccard coefficient(JC)

The Jaccard co-efficient is a metric that determines the proportion of similarities that exist between manually segmented ground truth images and the segmented output. If image A is the result of applying any segmentation method to it, and image B is the image that represents the ground truth, then the Jaccard coefficient may be written as

$$\text{Jaccard coefficient} = \frac{A \cap B}{A \cup B} \quad (29)$$

Fig. 11 depicts the comparison of JC of the suggested method with the conventional methods. Comparing the recommended way of MRI brain images to more conventional approaches, the figure clearly demonstrates that the suggested method has a higher JC.

4.4. Peal signal to noise ration (PSNR)

PSNR is useful for checking the noise level in an image in order to identify any decline in image quality that may have occurred. Fig. 12 depicts the PSNR comparison of the suggested method with the conventional methods. It shows the proposed method has a higher PSNR ratio when compared to the traditional methods. The present study's suggested strategy outperforms existing techniques with a PSNR score of 52.98 %.

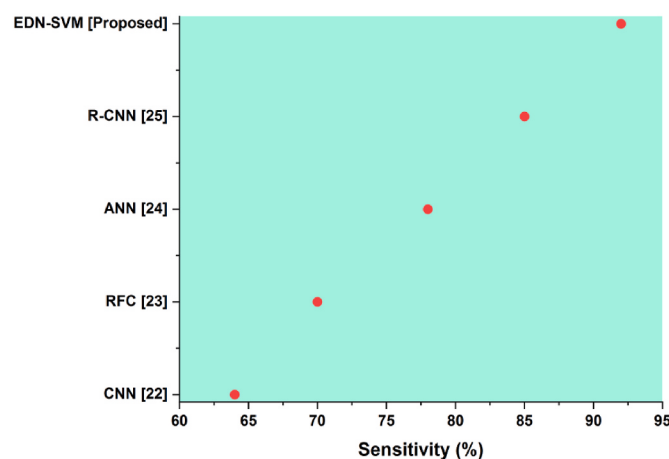


Fig. 13. Sensitivity comparison.

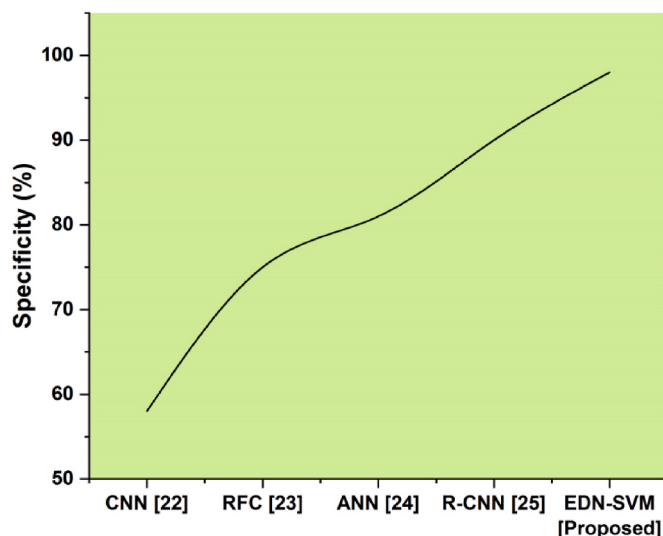


Fig. 14. Specificity comparison.

$$\text{PSNR} = 10 \log \frac{(255^2)}{\text{MSE}} \quad (30)$$

4.5. Sensitivity

The term “sensitivity” refers to the likelihood of a positive test on the assumption that it is positive. Another term for this is “true positive rate.” The sensitivity comparison between the proposed approach and the conventional methods is shown in [Fig. 13](#). It reveals that when compared to the sensitivity of the earlier approaches, the sensitivity of MRI images to classifying by the recommended approach EDN-SVM is superior. As compared to the current approaches, the suggested method has a high sensitivity of 92 %.

$$\text{Sensitivity} = \frac{TP}{(TP + FN)} \times 100 \quad (31)$$

4.6. Specificity

Specificity, also known as the true negative rate, is the likelihood of a negative test result under the assumption that the result is in fact negative. A comparison of the specificity of the suggested approach with that of the conventional methods is shown in [Fig. 14](#). The classification of MRI images reveals that the suggested method of EDN-SVM has a high degree of specificity when compared to the existing techniques. Evaluating the suggested method to the existing systems, it has a high specificity of 98 %.

$$\text{Specificity} = \frac{TN}{TN + FP} \times 100 \quad (32)$$

5. Discussion

The comparison of the suggested method to the existing models is shown in [Figs. 9–14](#). In order to conduct this inquiry, conventional methods such as CNN [22], RFC [23], ANN [24], and R-CNN [25] were used. The constraints of the approach that has previously been employed make the proposed strategy superior in terms of performance. The disadvantages of the present approaches include the ones that are listed below. The ANN is a model of hardware dependency, and it exhibits behaviour that cannot be described. In order to categorise tumour images, CNN requires a vast amount of training data. The fundamental drawback of RFC is that it may be rendered useless and unreasonably sluggish for use in real-time prediction when used with an excessively

large number of trees. While R-CNN cannot be done in real time since it takes around 47 s for each test image.

6. Conclusion

For the purpose of detecting brain tumors, the suggested EDN-SVM method proposes a novel method of image classification by establishing a direct link between all levels and ensuring that data is freely shared among them. Extensive simulations are conducted to test the effectiveness and viability of the suggested model. It has correctly identified the tumour image with a 97.93 % accuracy rate. Several benefits are shown by the data, suggesting that this model combination is worthwhile. To begin, the model automatically extracted the salient characteristics, making feature extraction far less time-consuming and arduous than it would have been with more conventional classifiers. Second, the suggested EDN-SVM model included the best features of deep NN and SVM, the two most well-known and widely-used classifiers for image recognition and classification. The following are the directions that the work going forward should take: (a) The algorithms that were created need to be included in the software that doctors use, and (b) the methodologies and procedures that were proposed in this research can only be used to grayscale photographs. Color images may be utilised to study the same difficulties and also work with 3D brain scans to obtain more effective brain tumour segmentation in future research.

Ethical compliance

No.

Declaration of competing interest

The authors declare that they have no known competing financial interests or personal relationships that could have appeared to influence the work reported in this paper.

Data availability

No data was used for the research described in the article.

Acknowledgments

There is no funding

References

- [1] E. Schulz, S.J. Gershman, The algorithmic architecture of exploration in the human brain, *Curr. Opin. Neurobiol.* 55 (2019) 7–14.
- [2] P.J. van Lonkhuijen, K.M. Klaver, J.S. Wefel, M.M. Sitskoorn, S.B. Schagen, K. Gehring, Interventions for cognitive problems in adults with brain cancer: a narrative review, *Eur. J. Cancer Care* 28 (3) (2019) e13088.
- [3] A. Del Dosso, J.P. Urenda, T. Nguyen, G. Quadrato, Upgrading the physiological relevance of human brain organoids, *Neuron* 107 (6) (2020) 1014–1028.
- [4] S.L. Fernandes, U.J. Tanik, V. Rajinikanth, K.A. Karthik, A reliable framework for accurate brain image examination and treatment planning based on early diagnosis support for clinicians, *Neural Comput. Appl.* 32 (20) (2020) 15897–15908.
- [5] Z.U. Rehman, S.S. Naqvi, T.M. Khan, M.A. Khan, T. Bashir, Fully automated multi-parametric brain tumour segmentation using superpixel based classification, *Expert Syst. Appl.* 118 (2019) 598–613.
- [6] Z.U. Rehman, M.S. Zia, G.R. Bojja, M. Yaqub, F. Jinchao, K. Arshid, Texture based localization of a brain tumor from MR-images by using a machine learning approach, *Med. Hypotheses* 141 (2020) 109705.
- [7] C. Kv, G.G. King, Brain tumour classification: a comprehensive systematic review on various constraints, in: *Computer Methods in Biomechanics and Biomedical Engineering: Imaging & Visualization*, 2022, pp. 1–13.
- [8] K. Rezaei, H. Agahi, A. Mahmoodzadeh, Multi-objective differential evolution-based ensemble method for brain tumour diagnosis, *IET Image Process.* 13 (9) (2019) 1421–1430.
- [9] R. Ezhilarasi, P. Varalakshmi, Tumor detection in the brain using faster R-CNN. In 2018 2nd international conference on I-smac (IoT in social, mobile, analytics and cloud)(I-smac) I-smac (IoT in social, mobile, analytics and cloud)(I-smac), 2018, in: *2nd International Conference on, IEEE*, 2018, August, pp. 388–392.

- [10] H. Mohsen, E.S.A. El-Dahshan, E.S.M. El-Horbaty, A.B.M. Salem, Classification using deep learning neural networks for brain tumors, *Future Computing and Informatics Journal* 3 (1) (2018) 68–71.
- [11] M. Siar, M. Teshnehab, Brain tumor detection using deep neural network and machine learning algorithm, in: 2019 9th International Conference on Computer and Knowledge Engineering (ICCKE), IEEE, 2019, October, pp. 363–368.
- [12] C.L. Choudhury, C. Mahanty, R. Kumar, B.K. Mishra, Brain tumor detection and classification using convolutional neural network and deep neural network, in: 2020 International Conference on Computer Science, Engineering and Applications (ICCSEA), IEEE, 2020, March, pp. 1–4.
- [13] M.A. Naser, M.J. Deen, Brain tumor segmentation and grading of lower-grade glioma using deep learning in MRI images, *Comput. Biol. Med.* 121 (2020) 103758.
- [14] M.K. Islam, M.S. Ali, M.S. Miah, M.M. Rahman, M.S. Alam, M.A. Hossain, Brain tumor detection in MR image using superpixels, principal component analysis and template based K-means clustering algorithm, *Machine Learning with Applications* 5 (2021) 100044.
- [15] T.A. Jemimma, Y.J. Vetharaj, Watershed algorithm based DAPP features for brain tumor segmentation and classification, in: 2018 International Conference on Smart Systems and Inventive Technology (ICSSIT), IEEE, 2018, December, pp. 155–158.
- [16] G. Hemanth, M. Janardhan, L. Sujihelen, Design and implementing brain tumor detection using machine learning approach, in: 2019 3rd International Conference on Trends in Electronics and Informatics (ICOEI), IEEE, 2019, April, pp. 1289–1294.
- [17] S.K. Chandra, M.K. Bajpai, Effective algorithm for benign brain tumor detection using fractional calculus, in: TENCON 2018-2018 IEEE Region 10 Conference, IEEE, 2018, October, pp. 2408–2413.
- [18] M. Gurbină, M. Lascu, D. Lascu, Tumor detection and classification of MRI brain image using different wavelet transforms and support vector machines, in: 2019 42nd International Conference on Telecommunications and Signal Processing (TSP), IEEE, 2019, July, pp. 505–508.
- [19] C. Sheela, G. Suganthi, Brain tumor segmentation with radius contraction and expansion based initial contour detection for active contour model, *Multimed. Tool. Appl.* 79 (33) (2020) 23793–23819.
- [20] S.J. Nanda, I. Gulati, R. Chauhan, R. Modi, U. Dhaked, A K-means-galactic swarm optimization-based clustering algorithm with Otsu's entropy for brain tumor detection, *Appl. Artif. Intell.* 33 (2) (2019) 152–170.
- [21] A. Wadhwa, A. Bhardwaj, V.S. Verma, A review on brain tumor segmentation of MRI images, *Magn. Reson. Imag.* 61 (2019) 247–259.
- [22] M.L. Martini, E.K. Oermann, Intraoperative brain tumour identification with deep learning, *Nat. Rev. Clin. Oncol.* 17 (4) (2020) 200–201.
- [23] M. Soltaninejad, G. Yang, T. Lambrou, N. Allinson, T.L. Jones, T.R. Barrick, F. A. Howe, X. Ye, Supervised learning based multimodal MRI brain tumour segmentation using texture features from supervoxels, *Comput. Methods Progr. Biomed.* 157 (2018) 69–84.
- [24] N. Arunkumar, M.A. Mohammed, S.A. Mostafa, D.A. Ibrahim, J.J. Rodrigues, V.H. de Albuquerque, Fully automatic model-based segmentation and classification approach for MRI brain tumor using artificial neural networks, *Concurrency Comput. Pract. Ex.* 32 (1) (2020) e4962.
- [25] K. Salçın, Detection and classification of brain tumours from MRI images using faster R-CNN, *Tehnički glasnik* 13 (4) (2019) 337–342.
- [26] M. Nazir, S. Shakil, K. Khurshid, Role of deep learning in brain tumor detection and classification (2015 to 2020): a review, *Comput. Med. Imag. Graph.* 91 (2021) 101940.
- [27] J. Amin, M. Sharif, M. Yasmin, S.L. Fernandes, A distinctive approach in brain tumor detection and classification using MRI, *Pattern Recogn. Lett.* 139 (2020) 118–127.
- [28] H.A. Khalil, S. Darwish, Y.M. Ibrahim, O.F. Hassan, 3D-MRI brain tumor detection model using modified version of level set segmentation based on dragonfly algorithm, *Symmetry* 12 (8) (2020) 1256.